

We are IntechOpen, the world's leading publisher of Open Access books Built by scientists, for scientists

5,800

Open access books available

142,000

International authors and editors

180M

Downloads

Our authors are among the

154

Countries delivered to

TOP 1%

most cited scientists

12.2%

Contributors from top 500 universities



WEB OF SCIENCE™

Selection of our books indexed in the Book Citation Index
in Web of Science™ Core Collection (BKCI)

Interested in publishing with us?
Contact book.department@intechopen.com

Numbers displayed above are based on latest data collected.
For more information visit www.intechopen.com



Waveguide Port Approach in EM Simulation of Microwave Antennas

Faik Bogdanov, Irina Chochia, Lily Svanidze and Roman Jobava

Abstract

This chapter generalizes a recently proposed MoM-based approach to waveguide port excitation (WPE) problems on arbitrary conducting and composite geometries. This approach combines the canonical aperture coupling approach with the EFIE-PMCHWT formulation for composite structures. Each WPE problem in this approach is divided into equivalent sub-problems for internal and external regions, which are solved using the MoM. Internal WPE problems are solved using waveguide modal expansion in the port plane, while external problems are solved using the equivalence principle to reduce these problems to the systems of algebraic equations for unknown electric and magnetic currents. The developed approach is validated on radiation and coupling problems for coaxial ports by comparing simulated results with those obtained by other approaches and measurements. An excellent agreement between the simulated and measured results is demonstrated. Finally, this approach is applied to practical EMC problems for microwave antennas fed by coaxial ports.

Keywords: coupling problem, coaxial port, equivalence principle, method of moments (MoM), waveguide modal expansion, waveguide port

1. Introduction

The excitation problem is of increasing importance at microwave frequencies [1]. Microwave antennas and other microwave devices are often fed by waveguides (rectangular, circular, and coaxial) or transmission lines (such as microstrips). In general, these devices are composite structures consisting of both conductive and dielectric elements. Therefore, the appropriate modeling of the waveguide excitation of such structures is of great interest. Such modeling in numerical methods is usually done by truncating the feed waveguide to create a waveguide port and formulate suitable boundary conditions (BC) imposed on the port. Such BCs should be able to launch an incident wave into the waveguide and absorb the reflected (in active mode) or received (in passive mode) wave without spurious reflections [2].

To date, most approaches to solving the waveguide port excitation (WPE) problem are based on volume discretization methods, such as the finite-element method (FEM) [1, 2], finite difference time domain (FDTD) [3–5], discontinuous Galerkin time-domain (DGTD) [6], contour integral method (CIM) [7], etc. Most of these works use various modal absorbing boundary conditions (MABC) [4, 5], developed for time-domain methods as termination conditions imposed on the port.

At present, many electromagnetic (EM) problems are solved using surface integral equations (SIE) together with the method of moments (MoM) [8]. Within the framework of SIE, the WPE problem was first formulated as an aperture coupling problem for a conducting geometry, and the MoM solution for magnetic currents was obtained in the presence of a short-circuited conductive sheet [9]. This approach was then modified using the pseudo-image method for magnetic currents in addition to electric currents [10]. Further, MoM was applied to the waveguide port problems [11] and antenna radiation problems with aperture port excitation [12]. However, until recently, a MoM-based solution to the WPE problem for arbitrary geometries has been poorly represented in the literature. In our recent works [13–15], such a solution was obtained for radiation and coupling problems for various types of geometries.

This chapter generalizes the recently proposed MoM-based approach to WPE problems [13–15] on arbitrary conducting and composite geometries. The obtained approach combines the canonical aperture coupling approach with the EFIE-PMCHWT formulation for composite structures [16–22]. Each WPE problem in this approach is divided into equivalent sub-problems for internal and external regions, which are solved using the MoM. The internal WPE problems are solved using waveguide modal expansion in the port plane, while the external problems are solved using the equivalence principle to reduce these problems to the systems of algebraic equations for unknown electric and magnetic currents. The obtained solution also considers the problem of material junctions between adjacent surfaces, considered in [19–22].

The developed approach is validated on radiation and coupling problems for coaxial ports by comparing the simulated results with those from other approaches and measurements. In addition, this approach is applied to practical EMC problems for microwave antennas fed by coaxial ports. The MoM calculations were performed using the TriD numerical code incorporated in the EMCoS Studio software package [23].

2. Waveguide port approach for conducting geometry

2.1 Dividing the original problem into equivalent problems

Figure 1a illustrates a canonical waveguide port problem for conducting geometry. This geometry consists of a semi-infinite waveguide 1 with perfect electric conducting (PEC) walls and a microwave structure 2, which is yet supposed to be conductive. We intend to create port P in waveguide 1 to divide the geometry into two regions (A and B) to truncate the mesh in the region A and impose appropriate termination conditions in the port plane.

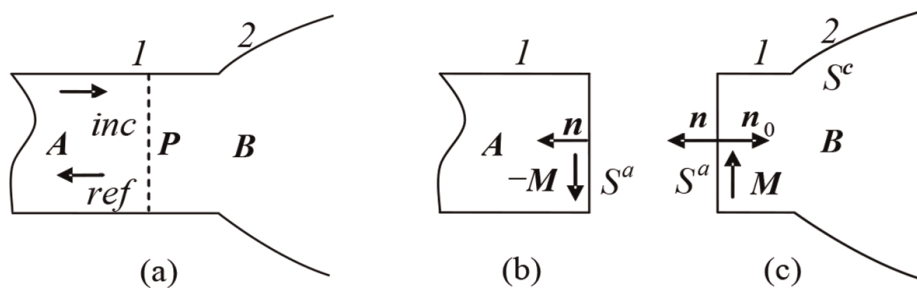


Figure 1. (a) Waveguide port problem for conducting geometry; (b) Equivalence for the internal region A ; (c) Equivalence for the external region B .

For this purpose, we follow the classical approach for the aperture problem [9] to divide the original problem into two equivalent problems, as shown in **Figure 1b** and **c**. We introduce a perfectly conducting surface S^a into the port plane P to separate regions A and B and consider two equivalent sub-problems: internal (for region A) and external (for region B). In addition, we introduce equivalent magnetic currents and \mathbf{M} on both sides of S^a to restore the tangential electric fields on the boundary surface S^a . Let us consider these equivalent problems separately.

2.2 Formulation of the internal equivalent problem

Consider an internal equivalent problem for the region A . The total EM field in the region A is composed of the incident field $\mathbf{E}^{inc}, \mathbf{H}^{inc}$ and the reflected field $\mathbf{E}^{ref}, \mathbf{H}^{ref}$ generated by magnetic currents in the presence of a conductor. According to the equivalence principle [24], these currents are related to the total electric field $\mathbf{E}_A^{S^a}$ on the port surface S^a by the relation:

$$-\mathbf{M} = -\mathbf{n} \times \mathbf{E}_A^{S^a} = \mathbf{n}_0 \times \mathbf{E}_A^{S^a} \quad (1)$$

where \mathbf{n} is the internal normal in the region A , and $\mathbf{n}_0 = -\mathbf{n}$ is the propagation direction of the incident wave.

Equation (1) relates the total electric field at the port surface S^a to magnetic currents depending on the geometric and material properties of the external region B . The internal equivalent problem is to find the modal expansion of the total EM field at the port surface S^a through these currents.

2.3 MoM solution of the internal equivalent problem

The total EM field in the region A on the port surface S^a can be generally written as the sum of the incident (+) and reflected (-) TEM (if exists), TE, and TM modes [2, 13]:

$$\mathbf{E}_A^{S^a} = (a_0^+ + a_0^-) \mathbf{e}_0^{TEM} + \sum_{s=1}^{N^{TE}} (a_s^+ + a_s^-) \mathbf{e}_s^{TE} + \sum_{s=1}^{N^{TM}} (b_s^+ + b_s^-) \mathbf{e}_s^{TM} \quad (2)$$

$$\begin{aligned} \mathbf{H}_A^{S^a} = & \frac{1}{Z} (a_0^+ - a_0^-) (\mathbf{n}_0 \times \mathbf{e}_0^{TEM}) + \sum_{s=1}^{N^{TE}} \frac{1}{Z_s^{TE}} (a_s^+ - a_s^-) (\mathbf{n}_0 \times \mathbf{e}_s^{TE}) \\ & + \sum_{s=1}^{N^{TM}} \frac{1}{Z_s^{TM}} (b_s^+ - b_s^-) (\mathbf{n}_0 \times \mathbf{e}_s^{TM}) \end{aligned} \quad (3)$$

where a_s^\pm and b_s^\pm are the mode amplitudes, \mathbf{e}_0^{TEM} , \mathbf{e}_s^{TE} and \mathbf{e}_s^{TM} are the transverse modal functions of TEM, TE and TM waves with wave impedances $Z = \sqrt{\mu/\epsilon}$, $Z_s^{TE} = \omega\mu/\gamma_s$ and $Z_s^{TM} = \gamma_s/\omega\epsilon$, respectively, ϵ and μ are the permittivity and permeability of the medium, γ_s is the propagation constant, and N^{TE} and N^{TM} are the numbers of accounted TE and TM modes, respectively.

Next, we use the MoM to relate the mode amplitudes of the reflected fields in (2), (3) to the magnetic currents \mathbf{M} . The port surface S^a is discretized into planar patches, and the unknown magnetic currents are approximated as

$$\mathbf{M} = \sum_{n=1}^{N^a} M_n \mathbf{f}_n \quad (4)$$

where \mathbf{f}_n are linear independent basis functions (BFs), M_n are unknown expansion current coefficients, and N^a is the number of these BF's on the surface S^a . Substituting now (4) and (2) into (1), multiplying both sides by $\mathbf{n}_0 \times \mathbf{e}_0^{TEM}$, $\mathbf{n}_0 \times \mathbf{e}_s^{TE}$ and $\mathbf{n}_0 \times \mathbf{e}_s^{TM}$, respectively, and integrating over the port surface S^a , we relate the amplitudes of the reflected waves with those of the incident waves and magnetic current coefficients:

$$a_s^- = -a_s^+ - \sum_{n=1}^{N^a} \frac{M_n T_{ns}}{R_s}, \quad b_s^- = -b_s^+ - \sum_{n=1}^{N^a} \frac{M_n T'_{ns}}{R'_s} \quad (s = 0, 1, 2, \dots) \quad (5)$$

where

$$T_{n0} = \int_{S_a} \mathbf{f}_n \cdot (\mathbf{n}_0 \times \mathbf{e}_0^{TEM}) dS', \quad T_{ns} = \int_{S_a} \mathbf{f}_n \cdot (\mathbf{n}_0 \times \mathbf{e}_s^{TE}) dS', \quad T'_{ns} = \int_{S_a} \mathbf{f}_n \cdot (\mathbf{n}_0 \times \mathbf{e}_s^{TM}) dS' \quad (6)$$

$$R_0 = \int_{S_a} (\mathbf{n}_0 \times \mathbf{e}_0^{TEM}) (\mathbf{n}_0 \times \mathbf{e}_0^{TEM}) dS', \quad R_s = \int_{S_a} (\mathbf{n}_0 \times \mathbf{e}_s^{TE}) (\mathbf{n}_0 \times \mathbf{e}_s^{TE}) dS', \quad (7)$$

$$R'_s = \int_{S_a} (\mathbf{n}_0 \times \mathbf{e}_s^{TM}) (\mathbf{n}_0 \times \mathbf{e}_s^{TM}) dS'.$$

Substitution of (5) into (2), (3) determines the total electric and magnetic fields on the port surface in region A through the still unknown magnetic currents.

2.4 Formulation of the external equivalent problem for conducting geometry

Consider now an external equivalent problem for conducting geometry. The scattered EM field in the external region B in **Figure 1c** of the conducting geometry is produced by electric currents \mathbf{J} flowing over surfaces S^a and S^c and equivalent magnetic currents \mathbf{M} at the surface S^a , which can be written as:

$$\mathbf{E}_B^{sc}(\mathbf{J}, \mathbf{M}) = L^{EJ} \mathbf{J} + L^{EM} \mathbf{M} \quad (8)$$

$$\mathbf{H}_B^{sc}(\mathbf{J}, \mathbf{M}) = L^{HJ} \mathbf{J} + L^{HM} \mathbf{M} \quad (9)$$

where L^{EJ} , L^{EM} , L^{HJ} and L^{HM} are the linear integro-differential operators of electric and magnetic fields applied to the electric and magnetic currents, respectively. Applying the boundary conditions for the tangential electric and magnetic fields on the surfaces S^a and S^c , we obtain the following system of integral equations for the unknown electric and magnetic currents \mathbf{J} and \mathbf{M}

$$\mathbf{E}_B^{sc}(\mathbf{J}, \mathbf{M})|_{\tan}^{S^a+S^c} = 0 \quad \text{just outside } S^a \quad (10)$$

$$\mathbf{H}_B^{sc}(\mathbf{J}, \mathbf{M})|_{\tan}^{S^a+S^c} = \mathbf{H}_A^{S^a}|_{\tan} \quad \text{just inside } S^a \quad (11)$$

2.5 MoM solution of the external equivalent problem for conducting geometry

To obtain the MoM solution to the BC (10) and (11), we consider, along with Eq. (4), the following expansion for an unknown electric current \mathbf{J} :

$$\mathbf{J} = \sum_{n=1}^{N^a+N^c} I_n \mathbf{f}_n, \quad (12)$$

where \mathbf{f}_n are the BFs taken the same as for the expansion of magnetic currents in (4), I_n are the unknown expansion current coefficients on the surfaces S^a and S^c , and N^a and N^c are the numbers of these BFs on these surfaces. Substitution of expansions (4) and (12) in (8) and (9) gives the following expressions for the EM field in region B :

$$\mathbf{E}_B^{sc}(\mathbf{J}, \mathbf{M}) = \sum_{n=1}^{N^a+N^c} I_n L^{EJ} \mathbf{f}_n + \sum_{n=1}^{N^a} M_n L^{EM} \mathbf{f}_n, \quad (13)$$

$$\mathbf{H}_B^{sc}(\mathbf{J}, \mathbf{M}) = \sum_{n=1}^{N^a+N^c} I_n L^{HJ} \mathbf{f}_n + \sum_{n=1}^{N^a} M_n L^{HM} \mathbf{f}_n. \quad (14)$$

Substituting now (3), (5), (13) and (14) into (10) and (11), introducing the boundary operators $\hat{L}^{JJ} = L^{EJ}|_{S^a+S^c}$, $\hat{L}^{JM} = L^{EM}|_{S^a+S^c}^{\text{outside}}$, $\hat{L}^{MJ} = L^{HJ}|_{S^a}^{\text{inside}}$ and $\hat{L}^{MM} = L^{HM}|_{S^a}$ and testing the resulting equations with appropriate weighting functions $\mathbf{w}_1(\mathbf{r})$, $\mathbf{w}_2(\mathbf{r})$, ..., $\mathbf{w}_m(\mathbf{r})$ leads to the following system of linear algebraic equations

$$\begin{bmatrix} [Z_{mn}^{JJ}] & [Z_{mn}^{JM}] \\ [Z_{mn}^{MJ}] & [Z_{mn}^{MM}] \end{bmatrix} \begin{bmatrix} [I_n] \\ [M_n] \end{bmatrix} = \begin{bmatrix} 0 \\ [V_m^W] \end{bmatrix} \quad (15)$$

with elements defined as:

$$Z_{mn}^{JJ} = -\langle \mathbf{w}_m, \hat{L}^{JJ} \mathbf{f}_n \rangle, \quad Z_{mn}^{JM} = -\langle \mathbf{w}_m, \left(\tilde{L}^{JM} + \frac{1}{2} \mathbf{n} \times \right) \mathbf{f}_n \rangle, \quad (16)$$

$$Z_{mn}^{MJ} = -\langle \mathbf{w}_m, \left(\tilde{L}^{MJ} + \frac{1}{2} \mathbf{n} \times \right) \mathbf{f}_n \rangle, \quad Z_{mn}^{MM} = -\langle \mathbf{w}_m, \hat{L}^{MM} \mathbf{f}_n \rangle + Q_{mn}^W, \quad (17)$$

$$Q_{mn}^W = \frac{\hat{T}_{m0}}{W} \frac{T_{n0}}{R_0} + \sum_{s=1}^{N^{TE}} \frac{\hat{T}_{ms}}{W_s^{TM}} \frac{T_{ns}}{R_s} + \sum_{s=1}^{N^{TM}} \frac{\hat{T}'_{ms}}{W_s^{TM}} \frac{T'_{ns}}{R'_s}, \quad (18)$$

$$V_m^W = -2 \left[\frac{\hat{T}_{m0}}{W} a_0^+ + \sum_{s=1}^{N^{TE}} \frac{\hat{T}_{ms}}{W_s^{TM}} a_s^+ + \sum_{s=1}^{N^{TM}} \frac{\hat{T}'_{ms}}{W_s^{TM}} b_s^+ \right], \quad (19)$$

where \tilde{L}^{JM} and \tilde{L}^{MJ} are the regular parts of the boundary operators \hat{L}^{JM} and \hat{L}^{MJ} , the notation $\langle \mathbf{w}, \mathbf{f} \rangle = \int_S \mathbf{w} \cdot \mathbf{f} dS$ is used for the scalar product, and

$$\hat{T}_{m0} = \int_{S_a} \mathbf{w}_m \cdot (\mathbf{n}_0 \times \mathbf{e}_0^{TEM}) dS', \quad \hat{T}_{ms} = \int_{S_a} \mathbf{w}_m \cdot (\mathbf{n}_0 \times \mathbf{e}_s^{TE}) dS', \quad \hat{T}'_{ms} = \int_{S_a} \mathbf{w}_m \cdot (\mathbf{n}_0 \times \mathbf{e}_s^{TM}) dS' \quad (20)$$

In the case of Galerkin’s procedure $\mathbf{w}_m = \mathbf{f}_m$, and coefficients (20) and (6) become the same. The MoM system (15) determines the solution to the waveguide port problem in the conducting geometry.

2.6 Validation of the developed approach for conducting geometry

The developed approach has been validated to simulate the scattering characteristics of a flanged coaxial line as proposed in [25–27]. Such structures are frequently used in biomedical engineering for non-destructive testing of various materials [25–27].

When modeling a coaxial line, it is convenient to choose the port plane at the output of the line to provide fast damping of evanescent waves. In this case, it can be assumed $N^{TE} = N^{TM} = 0$ in (2) and (3) to take taken into account only fundamental, TEM mode with the modal function $\mathbf{e}_0^{TEM} = \mathbf{e}_\rho / [\rho \cdot \ln(D/d)]$, where ρ is the radial distance, \mathbf{e}_ρ is the unit radial vector, and D and d are the outer and inner diameters of the coaxial waveguide.

Figure 2 shows a flanged coaxial line consisting of a coaxial waveguide section with an outer radius $D/2 = 4.725$ mm, an inner radius of $d/2 = 1.4364$ mm, and a length $L = 10$ mm, ended with a circular disc with a diameter $2R = 200$ mm. The bottom plane of the waveguide is accepted as a waveguide port, and the structure is excited in this port by TEM mode. To validate the developed approach for conducting geometry, we analyze the case when both the waveguide and outer space have the same permittivity $\epsilon_r = 2.05$.

Figure 3a and **b** show the magnitude and phase of the reflection coefficient at the end of the coaxial line used as the reference plane. We compare the simulation results obtained using the developed approach, the mode-matching technique [25], and the

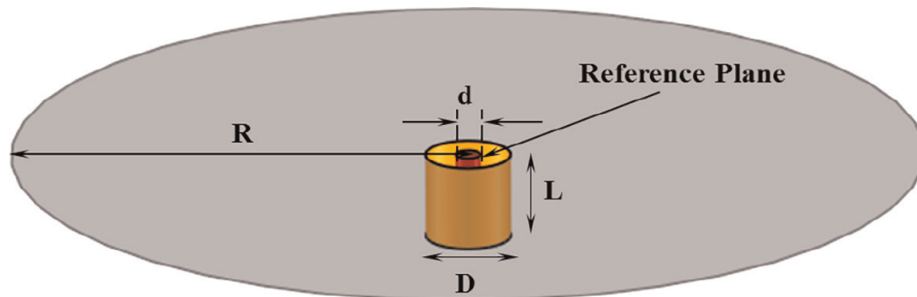


Figure 2. Geometry of open-ended coaxial line flanged with a circular disc: $D/2 = 4.725$ mm, $d/2 = 1.4364$ mm, $L = 10$ mm, $2R = 200$ mm, $\epsilon_r = 2.05$ inside and outside the line.

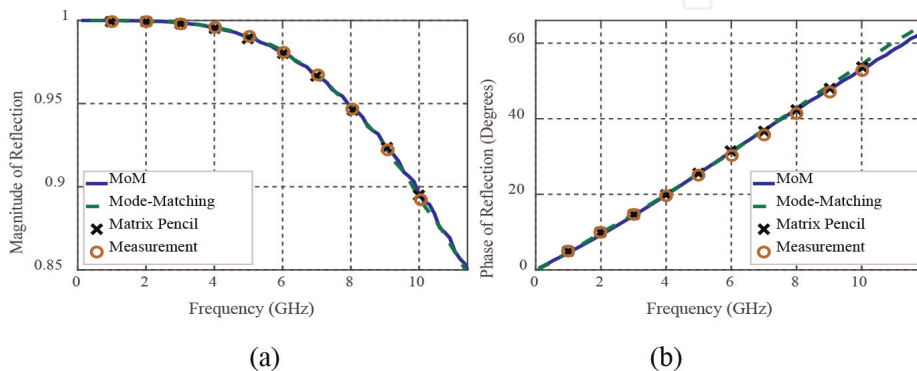


Figure 3. (a) Magnitude and (b) phase of the reflection coefficient versus the frequency of excitation at the end of the flanged coaxial line, calculated for various approaches.

matrix pencil method [26] with measurement data [27]. Note that infinite flanges are assumed in [25, 26]. Phase data conforms to the time convention $\exp(-i\omega t)$.

Comparison of various results shows excellent agreement between them. However, the phase characteristics obtained by our approach agree somewhat more accurately with the measurement data. Thus, the obtained results validate the developed approach to modeling a coaxial waveguide port for conducting geometries.

3. Waveguide port approach for composite geometry

3.1 Equivalent problems for composite geometry

Figure 4 shows the geometry of the problem, consisting of a composite structure composed of $k-1$ homogeneous regions D_i , $i = 1, 2, \dots, k-1$, located in the free space region D_0 and exposed to waveguide excitation from the waveguide region B , which will be considered as k -th region of the problem. The region D_k is a finite section of the waveguide, confined by the PEC walls, the port surface S^a , and the dielectric surface S_k^d , through which the structure is fed. The port surface S_a separates the region D_k (B) from the semi-infinite waveguide region A with incident waveguide excitation. In addition, each region D_i is excited, in general, by the incident field E_i^{inc} , H_i^{inc} .

To formulate the waveguide port excitation problem through the port surface S^a , we first consider the aperture coupling problem between the waveguide regions A and B [9]. Thus, we cover the port surface S^a with a PEC sheet and introduce equivalent magnetic currents $-M$ and M on both sides of S^a to divide the excitation problem into two different equivalence problems: the internal problem for region A , and the external problem for region B (D_k), as done in Section 2.1. Then, the internal equivalent problem is identical to that formulated in Section 2.2 and solved in Section 2.3. The external equivalent problem requires consideration of equivalent problems for each boundary surface in regions D_i , $i = 1, 2, \dots, k$, including the port surface S^a .

3.2 Formulation of the external equivalent problem for composite geometry

An external equivalent problem for composite geometry is reduced to a set of equivalent problems for each conducting and dielectric boundary S_i^c and S_i^d of free space region D_0 ($i = 0$), composite structure regions D_i ($i = 1, \dots, k-1$), and finite

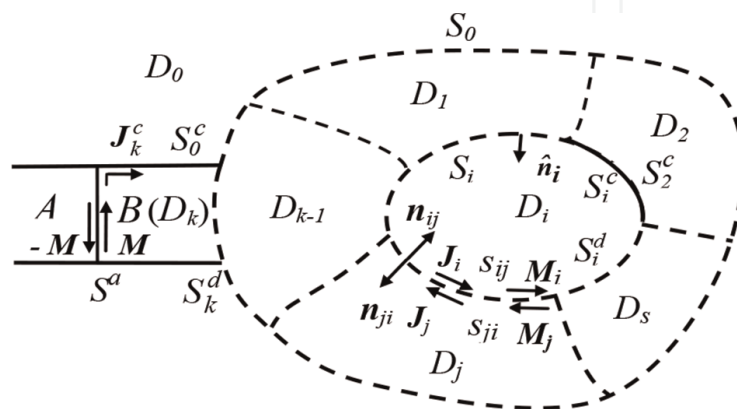


Figure 4. Waveguide port problem for composite geometry with waveguide excitation.

waveguide region D_k ($i = k$). In turn, each surface S_i^d comprises a set of boundary surfaces $s_{ij} = D_i \cap D_j$ ($i \neq j$), being the interfaces between the regions D_i and D_j .

Per the equivalence principle [24], the total EM field inside the i -th region D_i can be expressed as the sum of the incident field \mathbf{E}_i^{inc} , \mathbf{H}_i^{inc} and that induced by the total surface currents distributed over its boundary surface S_i and radiating into a homogeneous medium with constitutive parameters ε_i and μ_i of the region D_i . The total electric currents \mathbf{J}_i on the boundary surface S_i consist of conducting currents \mathbf{J}_i^c , flowing on the inner sides of conducting boundaries S_i^c , and equivalent electric currents \mathbf{J}_i^d , flowing on the inner sides of dielectric boundaries S_i^d . Magnetic currents in the region D_i are equivalent currents \mathbf{M}_i^d , flowing on dielectric boundaries S_i^d . In addition, in the waveguide region D_k there are equivalent magnetic currents \mathbf{M} on the port surface S^a .

Unknown electric and magnetic currents can be found using the boundary conditions at the conducting boundaries of the composite structure:

$$[\mathbf{E}_i^{inc} + \mathbf{E}_i^{sc}(\mathbf{J}_i^c, \mathbf{J}_i^d, \mathbf{M}_i^d)]|_{\tan}^{S_i^c} = 0, \quad i = 0, 1, \dots, k-1 \quad (21)$$

dielectric boundaries of regions D_i ($i, j = 0, 1, \dots, k, i \neq j$):

$$[\mathbf{E}_i^{inc} + \mathbf{E}_i^{sc}(\mathbf{J}_i^c, \mathbf{J}_i^d, \mathbf{M}_i^d, \mathbf{M}\delta_{ik})]|_{\tan}^{s_{ij}} = [\mathbf{E}_j^{inc} + \mathbf{E}_j^{sc}(\mathbf{J}_j^c, \mathbf{J}_j^d, \mathbf{M}_j^d, \mathbf{M}\delta_{jk})]|_{\tan}^{s_{ij}}, \quad (22)$$

$$[\mathbf{H}_i^{inc} + \mathbf{H}_i^{sc}(\mathbf{J}_i^c, \mathbf{J}_i^d, \mathbf{M}_i^d, \mathbf{M}\delta_{ik})]|_{\tan}^{s_{ij}} = [\mathbf{H}_j^{inc} + \mathbf{H}_j^{sc}(\mathbf{J}_j^c, \mathbf{J}_j^d, \mathbf{M}_j^d, \mathbf{M}\delta_{jk})]|_{\tan}^{s_{ij}}, \quad (23)$$

and on the port surface S_a and the conducting boundary S_k^c of the k -th region:

$$[\mathbf{E}_k^{inc} + \mathbf{E}_k^{sc}(\mathbf{J}_k^c, \mathbf{J}_k^d, \mathbf{M}_k^d, \mathbf{M})]|_{\tan}^{S^a+S_k^c} = 0 \quad \text{just outside } S^a \quad (24)$$

$$[\mathbf{H}_k^{inc} + \mathbf{H}_k^{sc}(\mathbf{J}_k^c, \mathbf{J}_k^d, \mathbf{M}_k^d, \mathbf{M})]|_{\tan}^{S^a} = \mathbf{H}_A^{S^a}|_{\tan} \quad \text{just inside } S^a, \quad (25)$$

where δ_{ik} is the Kronecker delta, which shows that magnetic currents \mathbf{M} radiate only in a waveguide region D_k . The magnetic field on the right-hand side of (25) is expressed by Eq. (3). The scattered EM fields in (21)–(25) can be expressed in terms of electric and magnetic currents \mathbf{J}_i and \mathbf{M}_i in the dielectric region D_i as

$$\mathbf{E}_i^{sc}(\mathbf{J}_i, \mathbf{M}_i) = -L_i^{EJ}(\mathbf{J}_i) - L_i^{EM}(\mathbf{M}_i) \quad (26)$$

$$\mathbf{H}_i^{sc}(\mathbf{J}_i, \mathbf{M}_i) = -L_i^{HJ}(\mathbf{J}_i) - L_i^{HM}(\mathbf{M}_i) \quad (27)$$

where L_i^{EJ} , L_i^{EM} , L_i^{HJ} and L_i^{HM} are linear integro-differential operators of EM fields applied to currents radiated in the i -th region. It can also be shown [19–22] that the equivalent currents on opposite sides of the dielectric boundaries are related as:

$$\mathbf{J}_i^d = -\mathbf{J}_j^d, \quad \mathbf{M}_i^d = -\mathbf{M}_j^d \quad \text{on } s_{ij} \quad (28)$$

Equation (21)–(25) together with relations (26)–(28) and expansions (3) represent the general (EFIE-PMCHWT) form of integral equations for a composite structure with an arbitrary excitation, including the waveguide port.

3.3 MoM solution of the external equivalent problem for composite geometry

To solve the coupled system of integral Eqs. (21)–(28), we use the MoM to discretize the geometry of all boundary surfaces of the regions D_i ($i=1, \dots, k$) into the planar patches and to consider the following expansions for the unknown currents:

$$\mathbf{J}_k^c = \sum_{n=1}^{N^a+N_k^c} I_n^c \mathbf{f}_n, \quad \mathbf{M} = \sum_{n=1}^{N_a} M_n, \quad [\mathbf{J}_i^c]_{i=0}^{k-1} = \sum_{n=1}^{N^c} I_n^c \mathbf{f}_n, \quad (29)$$

$$[\mathbf{J}_i^d]_{i=0}^k = \sum_{n=1}^{N^d} I_n^d \mathbf{f}_n, \quad [\mathbf{M}_i^d]_{i=0}^k = \sum_{n=1}^{N^d} M_n^d \mathbf{f}_n, \quad (30)$$

where \mathbf{f}_n are the suitable BFs, I_n^c , M_n , I_n^C , I_n^d and M_n^d are the unknown expansion current coefficients, and N^a , N_k^c , N^C and N^d are the numbers of BFs on the surfaces

S^a , S_k^c , $[S_i^c]_{i=0}^{k-1}$, if any, and $[S_i^d]_{i=0}^{k-1}$, respectively. Expansions (29) and (30) take into account relations (28) for unknown equivalent currents on opposite sides of the dielectric boundaries. They also consider the ratios for adjacent currents at material junctions, which are the boundaries between several media [22].

Substituting (29) and (30) into (21)–(25) taking into account (3), (5), (26)–(28) and testing the resulting equations with weighting functions $\mathbf{w}_1(\mathbf{r})$, $\mathbf{w}_2(\mathbf{r})$, ..., $\mathbf{w}_m(\mathbf{r})$, defined in the range of the respective boundary operators, we obtain the following MoM system of linear algebraic equations:

$$\begin{bmatrix} [Z_{mn}^{J^c J^c}] & [Z_{mn}^{J^c M}] & 0 & [Z_{mn}^{J^c J^d}] & [Z_{mn}^{J^c M^d}] \\ [Z_{mn}^{M J^c}] & [Z_{mn}^{MM} + Q_{mn}^W] & 0 & [Z_{mn}^{M J^d}] & [Z_{mn}^{MM^d}] \\ 0 & 0 & [Z_{mn}^{J^C J^C}] & [Z_{mn}^{J^C J^d}] & [Z_{mn}^{J^C M^d}] \\ [Z_{mn}^{J^d J^c}] & [Z_{mn}^{J^d M}] & [Z_{mn}^{J^d J^C}] & [Z_{mn}^{J^d J^d}] & [Z_{mn}^{J^d M^d}] \\ [Z_{mn}^{M^d J^c}] & [Z_{mn}^{M^d M}] & [Z_{mn}^{M^d J^C}] & [Z_{mn}^{M^d J^d}] & [Z_{mn}^{M^d M^d}] \end{bmatrix} \begin{bmatrix} [I_n^c] \\ [M_n] \\ [I_n^C] \\ [I_n^d] \\ [M_n^d] \end{bmatrix} = \begin{bmatrix} [V_m^c] \\ [V_m^M + V_m^W] \\ [V_m^C] \\ [V_m^d] \\ [V_m^{Hd}] \end{bmatrix} \quad (31)$$

where the matrix elements are defined as $Z_{mn}^{\alpha\beta} = -\langle \mathbf{w}_m, \hat{L}^{\alpha\beta} \mathbf{f}_n \rangle$, $\hat{L}^{\alpha\beta}$ is the respective boundary integral operator, superscripts $\alpha, \beta = \{J^c, M, J^C, J^d, M^d\}$; $V_m^c = \langle \mathbf{w}_m, \mathbf{E}_k^{inc} \rangle$, $V_m^M = \langle \mathbf{w}_m, \mathbf{H}_k^{inc} \rangle$, $[V_m^C]_i = \langle \mathbf{w}_m, \mathbf{E}_i^{inc} \rangle$, $[V_m^d]_{ij} = \langle \mathbf{w}_m, \mathbf{E}_i^{inc} - \mathbf{E}_j^{inc} \rangle$, $[V_m^{Hd}]_{ij} = \langle \mathbf{w}_m, \mathbf{H}_i^{inc} - \mathbf{H}_j^{inc} \rangle$ are the voltage elements due to the incident wave in i -th and j -th media, and the elements Q_{mn}^W and V_m^W are the same as those expressed by (18) and (19) and determine the additional inclusions in the matrix and voltage elements due to the waveguide ports.

The MoM system (31) generalizes the solution (15) of the canonical waveguide port problem to the case of composite geometry. In the structure of the MoM matrix of this solution, blocks of waveguide excitation, complex structure, and couplings between these objects through dielectric interfaces are clearly seen.

3.4 Validation of the developed approach for composite geometry

The developed approach has been validated to simulate the scattering characteristics of a single monopole antenna, fed by waveguide excitation from a flanged coaxial line with dielectric filling. **Figure 5a** shows a schematic view of such antenna with a height $h_a = 10$ mm placed above a square metallic plate of $20 \text{ mm} \times 20 \text{ mm}$, which serves as a reflector. The coaxial line has an outer diameter $D = 6.98$ mm, an inner diameter $d = 2$ mm, and a length $h_b = 15$ mm. The line bottom end is accepted as a waveguide port, and the input impedance of the antenna at this port is simulated for various dielectric fillings of the line.

Figure 6 shows a comparison of the input impedances, calculated by the developed approach for the model of **Figure 5a** with $\epsilon_r = 1.0001$, by the WPE approach for the conducting model of **Figure 5b**, and by discontinuous Galerkin time-domain (DGTD) method [28]. An excellent agreement between the obtained results is seen, which confirms the equivalence and correctness of both WPE approaches (for conducting and composite geometries) for very low dielectric fillings of coaxial lines.

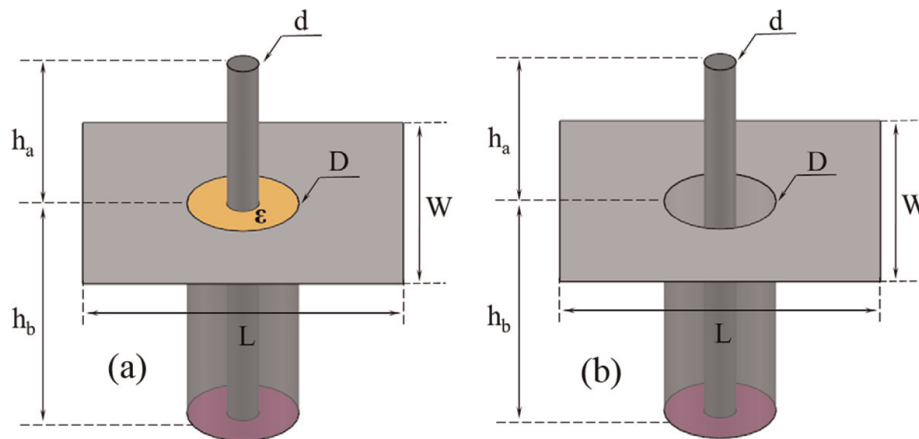


Figure 5. Single monopole antenna fed by a flanged coaxial line: (a) with dielectric filling; (b) without dielectric filling.

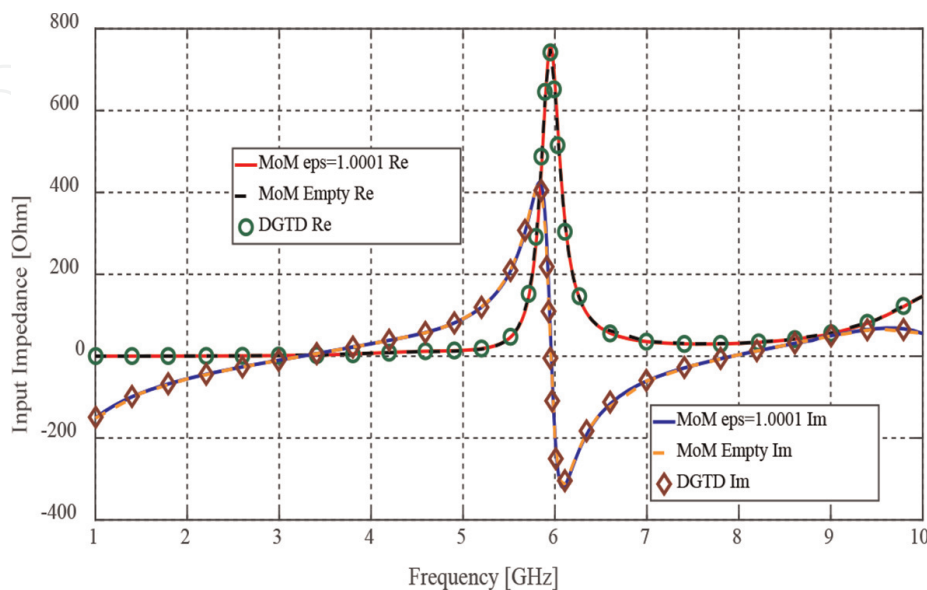


Figure 6. Comparison of the input impedances of a monopole antenna in the port plane, calculated by the MoM for $\epsilon_r = 1.0001$ and $\epsilon_r = 1$ with DGTD method.

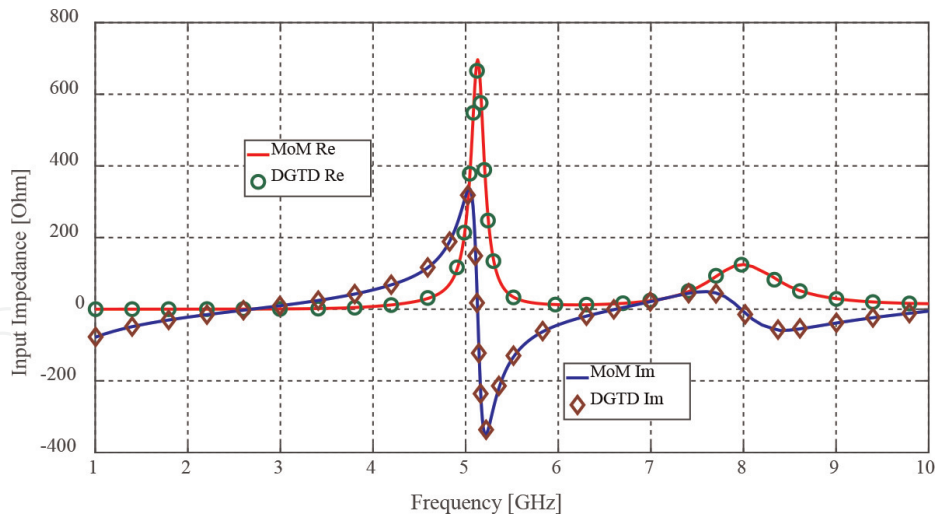


Figure 7. Comparison of the input impedances of a monopole antenna in the port plane for the dielectric filling of a coaxial line $\epsilon_r = 2.25$ calculated by MoM and DGTD method.

Figure 7 shows a comparison of the input impedances, calculated for the model of **Figure 5a** with $\epsilon_r = 2.25$ using the developed approach and DGTD method. An excellent agreement between both results is seen, which validates our approach to treat arbitrary dielectric and geometric parameters of composite structures with waveguide port excitation.

Comparison of **Figures 6** and **7** shows that the use of dielectric filling of the coaxial line shifts the resonances of the input impedance to lower frequencies. In addition, this leads to a change in the line's characteristic impedance from 75Ω in **Figure 6** to 50Ω in **Figure 7**. Thus, the developed WPE approach for composite geometries covers a wider area of geometries and provides more control over the characteristics of the analyzed structures.

4. Waveguide port approach in coupling problems

4.1 Problem formulation

Consider the coupling problem between several composite structures fed by waveguide excitations. Although each structure can be formed from an arbitrary number of dielectric regions, for simplicity, we will consider only one-region structures with composite (dielectric and conducting) boundaries. **Figure 8** shows the geometry of the problem consisting of N waveguides W_i radiating into dielectric regions D_i , $i = 1, 2, \dots, N$, surrounded by closed surfaces S_{D_i} with partially conducting boundaries $S_{D_i}^c$ and inward unit normal \mathbf{n}_{D_i} . Waveguides W_i are filled, in general, by dielectrics with permittivities ϵ_i and permeabilities μ_i , and the regions D_i are filled by dielectrics with parameters ϵ_{D_i} and μ_{D_i} . An outer space region D_0 is a free space with material parameters ϵ_0, μ_0 .

The waveguide ports P_i in cross-sections S_i^a divide the waveguides W_i into semi-infinite regions A_i and finite regions B_i to truncate the mesh in regions A_i with incident waveguide excitation and act as excitation sources of composite regions D_i through the dielectric boundaries $S_{D_i B_i}^d$ between the regions D_i and B_i . Each region B_i , D_i and D_0 is also excited, for generality, by the impressed EM field $\mathbf{E}_\alpha^{inc}, \mathbf{H}_\alpha^{inc}$, $\alpha = B_i, D_i, D_0$.

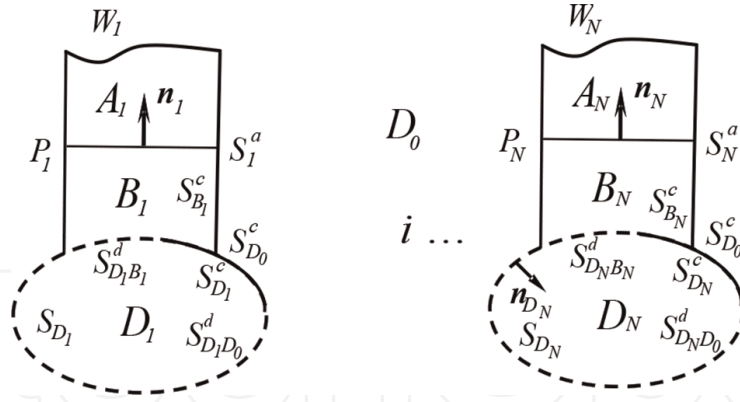


Figure 8.
Geometry of the problem.

To formulate the waveguide port excitation problems through the port surfaces S_i^a , we consider the aperture coupling problems between the regions A_i and B_i to divide an original problem into two sets of equivalence problems: internal problems for regions A_i and external problems for regions B_i , D_i and D_0 . For this purpose, we cover the port surfaces S_i^a with PEC sheets and introduce equivalent magnetic currents $-\mathbf{M}_i$ and \mathbf{M}_i on both sides of S_i^a to restore tangential electric fields on the port surfaces S_i^a .

4.2 Solution of the internal equivalent problem

The internal equivalent problems for the considered geometry are similar to those formulated in Section 2.2 and implemented in Section 2.3. According to the equivalence principle [24], the magnetic currents in the regions A_i are related to the total electric field $\mathbf{E}_{A_i}^{S_i^a}$ on the port surface S_i^a by the relation:

$$-\mathbf{M}_i = -\mathbf{n}_i \times \mathbf{E}_{A_i}^{S_i^a} = \mathbf{n}_{0i} \times \mathbf{E}_{A_i}^{S_i^a} \quad (32)$$

where \mathbf{n}_i is an inward normal in the region A_i , and $\mathbf{n}_{0i} = -\mathbf{n}_i$ is the propagation direction of the incident wave. Thus, the solution of the internal problem is expressed by formulas analogous to those obtained in Section 2.3 with adding the index i , when necessary.

4.3 Formulation of the external equivalent problem

When considering the external equivalent problem, let $S_{B_i}^c$ be the conducting boundary of the region B_i , including the inner sides of the waveguide walls and the conductive part of the boundary surface between the regions B_i and D_i ; $S_{D_i}^c$ is the conductive part of the boundary surface S_{D_i} , and $S_{D_0}^c$ is the conducting boundary of the region D_0 , including the outer sides of the waveguide walls and all conducting boundaries between the regions D_0 and D_i . Further, $S_{D_i B_i}^d$ is the dielectric boundary between the regions D_i and B_i , and $S_{D_i D_0}^d$ is the dielectric boundary between the regions D_i and D_0 . Per the equivalence principle [24], the dielectric boundaries between different regions can be replaced by oppositely directed equivalent electric and magnetic currents flowing on both sides of the dielectric interfaces.

The EM field in the waveguide region B_i is created by electric currents $\mathbf{J}_{B_i}^c$ flowing along the port surface S_i^a and conducting surface $S_{B_i}^c$, equivalent electric and magnetic

currents $-\mathbf{J}_{D_i B_i}^d$ and $-\mathbf{M}_{D_i B_i}^d$ flowing along the dielectric interfaces $S_{D_i B_i}^d$, and equivalent magnetic currents \mathbf{M}_i flowing along the port surface S_i^a . The EM field in the region D_i is created by electric currents $\mathbf{J}_{D_i}^c$ flowing along the conducting surfaces $S_{D_i}^c$, equivalent currents $\mathbf{J}_{D_i B_i}^d$ and $\mathbf{M}_{D_i B_i}^d$ flowing on dielectric boundaries $S_{D_i B_i}^d$ between the regions D_i and B_i , and equivalent currents $\mathbf{J}_{D_i D_0}^d$ and $\mathbf{M}_{D_i D_0}^d$ flowing on dielectric boundaries $S_{D_i D_0}^d$ between the regions D_i and D_0 . The field in the free space region D_0 is created by electric currents $\mathbf{J}_{D_0}^c$ flowing along the total conducting boundary of the region D_0 , and equivalent currents $-\mathbf{J}_{D_i D_0}^d$ and $-\mathbf{M}_{D_i D_0}^d$ at dielectric boundaries between the regions D_i and D_0 .

The unknown currents $\mathbf{J}_{B_i}^c$, \mathbf{M}_i , $\mathbf{J}_{D_i}^c$, $\mathbf{J}_{D_i B_i}^d$, $\mathbf{M}_{D_i B_i}^d$, $\mathbf{J}_{D_0}^c$, $\mathbf{J}_{D_i D_0}^d$, $\mathbf{M}_{D_i D_0}^d$ can be found from the boundary conditions on the port surface and the conducting boundaries of the waveguide region B_i :

$$\left[\mathbf{E}_{B_i}^{inc} + \mathbf{E}_{B_i}^{sc} \left(\mathbf{J}_{B_i}^c, \mathbf{M}_i, -\mathbf{J}_{D_i B_i}^d, -\mathbf{M}_{D_i B_i}^d \right) \right] \Big|_{\tan}^{S_i^a + S_i^c} = 0 \quad \text{just outside } S_i^a \quad (33)$$

$$\left[\mathbf{H}_{B_i}^{inc} + \mathbf{H}_{B_i}^{sc} \left(\mathbf{J}_{B_i}^c, \mathbf{M}_i, -\mathbf{J}_{D_i B_i}^d, -\mathbf{M}_{D_i B_i}^d \right) \right] \Big|_{\tan}^{S_i^a} = \mathbf{H}_{A_i}^{S_i^a} \Big|_{\tan} \quad \text{just inside } S_i^a, \quad (34)$$

and the boundary conditions on the conducting and dielectric boundaries of the regions D_i and D_0 :

$$\left[\mathbf{E}_{D_i}^{inc} + \mathbf{E}_{D_i}^{sc} \left(\mathbf{J}_{D_i}^c, \mathbf{J}_{D_i B_i}^d, \mathbf{M}_{D_i B_i}^d, \mathbf{J}_{D_i D_0}^d, \mathbf{M}_{D_i D_0}^d \right) \right] \Big|_{\tan} = 0 \quad \text{on } S_{D_i}^c \quad (35)$$

$$\left[\mathbf{E}_{B_i}^{inc} + \mathbf{E}_{B_i}^{sc} \left(\mathbf{J}_{B_i}^c, \mathbf{M}_i, -\mathbf{J}_{D_i B_i}^d, -\mathbf{M}_{D_i B_i}^d \right) \right] \Big|_{\tan} = \quad \text{on } S_{D_i B_i}^d \quad (36)$$

$$\left[\mathbf{E}_{D_i}^{inc} + \mathbf{E}_{D_i}^{sc} \left(\mathbf{J}_{D_i}^c, \mathbf{J}_{D_i B_i}^d, \mathbf{M}_{D_i B_i}^d, \mathbf{J}_{D_i D_0}^d, \mathbf{M}_{D_i D_0}^d \right) \right] \Big|_{\tan} = \quad \text{on } S_{D_i B_i}^d \quad (37)$$

$$\left[\mathbf{H}_{D_i}^{inc} + \mathbf{H}_{D_i}^{sc} \left(\mathbf{J}_{D_i}^c, \mathbf{M}_i, -\mathbf{J}_{D_i B_i}^d, -\mathbf{M}_{D_i B_i}^d \right) \right] \Big|_{\tan} = \quad \text{on } S_{D_i B_i}^d \quad (37)$$

$$\left[\mathbf{H}_{D_i}^{inc} + \mathbf{H}_{D_i}^{sc} \left(\mathbf{J}_{D_i}^c, \mathbf{J}_{D_i B_i}^d, \mathbf{M}_{D_i B_i}^d, \mathbf{J}_{D_i D_0}^d, \mathbf{M}_{D_i D_0}^d \right) \right] \Big|_{\tan} = \quad \text{on } S_{D_i B_i}^d \quad (37)$$

$$\left[\mathbf{E}_{D_0}^{inc} + \sum_{i=1}^N \mathbf{E}_{D_0}^{sc} \left(\mathbf{J}_{D_0}^c, -\mathbf{J}_{D_i D_0}^d, -\mathbf{M}_{D_i D_0}^d \right) \right] \Big|_{\tan} = 0 \quad \text{on } S_{D_0}^c \quad (38)$$

$$\left[\mathbf{E}_{D_i}^{inc} + \mathbf{E}_{D_i}^{sc} \left(\mathbf{J}_{D_i}^c, \mathbf{J}_{D_i B_i}^d, \mathbf{M}_{D_i B_i}^d, \mathbf{J}_{D_i D_0}^d, \mathbf{M}_{D_i D_0}^d \right) \right] \Big|_{\tan} = \quad \text{on } S_{D_i D_0}^d \quad (39)$$

$$\left[\mathbf{E}_{D_0}^{inc} + \mathbf{E}_{D_0}^{sc} \left(\mathbf{J}_{D_0}^c \right) + \sum_{i=1}^N \mathbf{E}_{D_0}^{sc} \left(-\mathbf{J}_{D_i D_0}^d, -\mathbf{M}_{D_i D_0}^d \right) \right] \Big|_{\tan} = \quad \text{on } S_{D_i D_0}^d \quad (39)$$

$$\left[\mathbf{H}_{D_i}^{inc} + \mathbf{H}_{D_i}^{sc} \left(\mathbf{J}_{D_i}^c, \mathbf{J}_{D_i B_i}^d, \mathbf{M}_{D_i B_i}^d, \mathbf{J}_{D_i D_0}^d, \mathbf{M}_{D_i D_0}^d \right) \right] \Big|_{\tan} = \quad \text{on } S_{D_i D_0}^d \quad (40)$$

$$\left[\mathbf{H}_{D_0}^{inc} + \mathbf{H}_{D_0}^{sc} \left(\mathbf{J}_{D_0}^c \right) + \sum_{i=1}^N \mathbf{H}_{D_0}^{sc} \left(-\mathbf{J}_{D_i D_0}^d, -\mathbf{M}_{D_i D_0}^d \right) \right] \Big|_{\tan} = \quad \text{on } S_{D_i D_0}^d \quad (40)$$

The scattered EM fields in (33)–(40) are related to the equivalent electric and magnetic currents by Eqs. (26) and (27). After substituting (26) and (27) into (35)–(40), Eqs. (35)–(40) represent a coupled system of integral equations in terms of unknown currents for solving the coupling problem between several composite structures.

4.4 MoM solution of the external equivalent problem

To solve the boundary problem (35)–(40), we use the following MoM expansions for the unknown currents:

$$\left[\mathbf{J}_{B_i}^c \right]_{i=1}^N = \sum_{n=1}^{N^a + N_B^c} I_n^{cB} \mathbf{f}_n, \left[\mathbf{M}_i \right]_{i=1}^N = \sum_{n=1}^{N^a} M_n \mathbf{f}_n, \left[\mathbf{J}_{D_i}^c \right]_{i=1}^N = \sum_{n=1}^{N_D^c} I_n^{cD} \mathbf{f}_n, \mathbf{J}_{D_0}^c = \sum_{n=1}^{N_{D_0}^c} I_n^{cD_0} \mathbf{f}_n, \quad (41)$$

$$\left[\mathbf{J}_{D_i B_i}^d, \mathbf{J}_{D_i D_0}^d \right]_{i=1}^N = \sum_{n=1}^{N^d} I_n^d \mathbf{f}_n, \left[\mathbf{M}_{D_i B_i}^d, \mathbf{M}_{D_i D_0}^d \right]_{i=1}^N = \sum_{n=1}^{N^d} M_n^d \mathbf{f}_n, \left[\mathbf{M}_i \right]_{i=1}^N = \sum_{n=1}^{N^a} M_n \mathbf{f}_n \quad (42)$$

where \mathbf{f}_n are the suitable BFs, $I_n^{cB}, I_n^{cD}, I_n^{cD_0}, I_n^d, M_n^d$ and M_n are the unknown expansion current coefficients, and $N^a, N_B^c, N_D^c, N_{D_0}^c$ and N^d are the numbers of these BFs on the surfaces $[S_i^a]_{i=1}^N, [S_{B_i}^c]_{i=1}^N, [S_{D_i}^c]_{i=1}^N, S_{D_0}^c$ and $[S_{D_i B_i}^d, S_{D_i D_0}^d]_{i=1}^N$, respectively. Substituting now (41) and (42) into (35)–(40) with an accounting of (3), (5), and (26) and (27) for each i -th region and testing the obtained equations with weighting functions $\mathbf{w}_1(\mathbf{r}), \mathbf{w}_2(\mathbf{r}), \dots, \mathbf{w}_m(\mathbf{r})$, defined in the range of the respective boundary operators, we obtain the following MoM system of linear algebraic equations:

$$\begin{bmatrix} Z_{B_i B_i}^{J^c} & Z_{B_i}^{J^c M} & 0 & 0 & Z_{B_i}^{J^c J^d} & Z_{B_i}^{J^c M^d} \\ Z_{B_i}^{M J^c} & Z^{M M} + Q^W & 0 & 0 & Z_{B_i}^{M J^d} & Z^{M M^d} \\ 0 & 0 & Z_{D_i}^{J^c J^c} & 0 & Z_{D_i}^{J^c J^d} & Z_{D_i}^{J^c M^d} \\ 0 & 0 & 0 & Z_{D_0}^{J^c J^c} & Z_{D_0}^{J^c J^d} & Z_{D_0}^{J^c M^d} \\ Z_{D_i}^{J^d J^c} & Z_{D_i}^{J^d J^c} & Z_{D_i}^{J^d J^c} & Z_{D_i}^{J^d J^c} & Z_{D_i}^{J^d J^d} & Z_{D_i}^{J^d M^d} \\ Z_{D_i}^{M^d J^c} & Z_{D_i}^{M^d M} & Z_{D_i}^{M^d J^c} & Z_{D_i}^{M^d J^c} & Z_{D_i}^{M^d J^d} & Z_{D_i}^{M^d M^d} \end{bmatrix} \begin{bmatrix} I^{cB} \\ M \\ I^{cD} \\ I^{cD_0} \\ I^d \\ M^d \end{bmatrix} = \begin{bmatrix} V^{cB} \\ V^M + V^W \\ V^{cD} \\ V^{cD_0} \\ V^d \\ V^{Hd} \end{bmatrix} \quad (43)$$

where the elements of the block matrices are defined as: $Z_{mn}^{\alpha\beta} = -\langle \mathbf{w}_m, \hat{L}_i^{\alpha\beta} \mathbf{f}_n \rangle$, $\hat{L}_i^{\alpha\beta}$ is the respective boundary integral operator, superscripts $\alpha, \beta = \{J_B^c, M, J_D^c, J_{D_0}^c, J^d, M^d\}$, voltage elements are defined in the same way as in Eq. (31), and the elements of the block matrices Q^W and V^W are expressed by (18) and (19) for each i -th feeding waveguide and determine the additional inclusions in the matrix and voltage elements due to the waveguide ports. The MoM system (43) defines a solution to the coupling problem between several composite geometries. In the structure of the MoM matrix of this solution, blocks of waveguide excitations, complex geometries, and couplings between them are clearly seen.

4.5 Validation of the developed approach for coupling problems

The developed approach has been validated on a two-element antenna array fed by coaxial waveguide ports by comparing the simulation results obtained using the developed MoM approach and the DGTD method [28]. **Figure 9** shows a schematic

view of two identical monopole antennas flanged over the PEC plate and fed by coaxial waveguides with generally different diameters and dielectric fillings. The monopoles located at a distance $L_a = 40$ mm from each other have the same height $h_a = 10$ mm above the PEC plate with a width $W = 40$ mm and a length $L = 80$ mm, which serves as a reflector. Coaxial waveguides have the same inner diameter $d_1 = d_2 = 2$ mm, but generally different outer diameters D_1 and D_2 and relative permittivities ϵ_1 and ϵ_2 . The depth of each coaxial waveguide under the flange is $h_b = 15$ mm, and its end is taken as the reference plane of the waveguide port.

Figure 10 shows the real and imaginary parts of the transmission coefficient $S_{21} = a_{02}^-/a_{01}^+$ between waveguide ports 1 and 2 with the same radii and dielectric fillings: $D_1/2 = D_2/2 = 6.65$ mm, and $\epsilon_{r1} = \epsilon_{r2} = 5.17$, which leads to the same characteristic impedances: $Z_{c1} = Z_{c2} = 50 \Omega$. The developed MoM approach and the DGTD method are compared. The first antenna in these simulations is considered active, and the second is passive. Comparison of these results shows very good agreement between them over a wide frequency range from 1 GHz up to 10 GHz. This validates the developed approach in modeling coupling problems for coaxial waveguide ports with the same characteristic impedance.

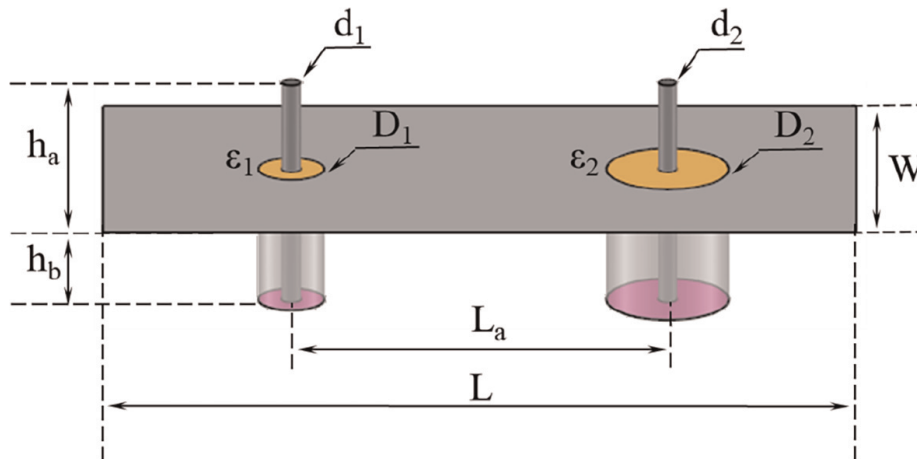


Figure 9. Schematic view of an array of two identical monopole antennas fed by coaxial waveguides and flanged above the PEC plate.

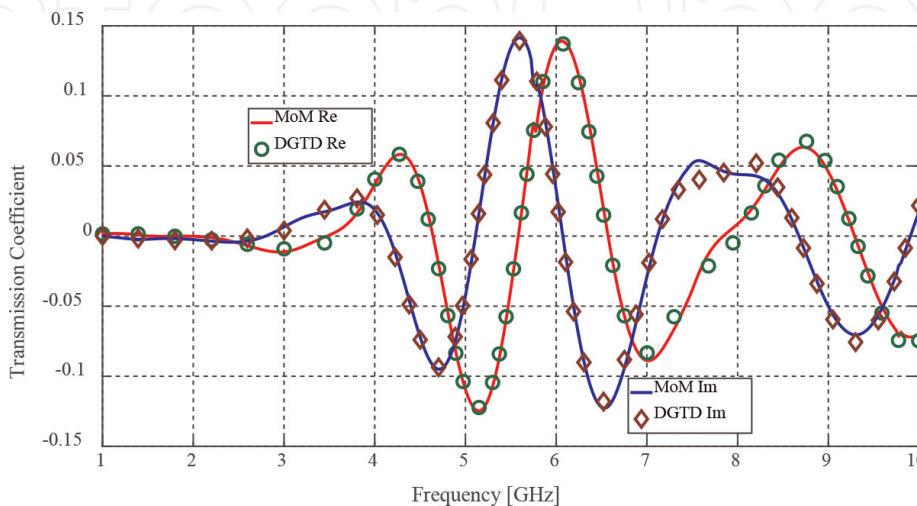


Figure 10. Transmission coefficient between the antenna array waveguide ports with the same parameters of the feeding coaxial waveguides.

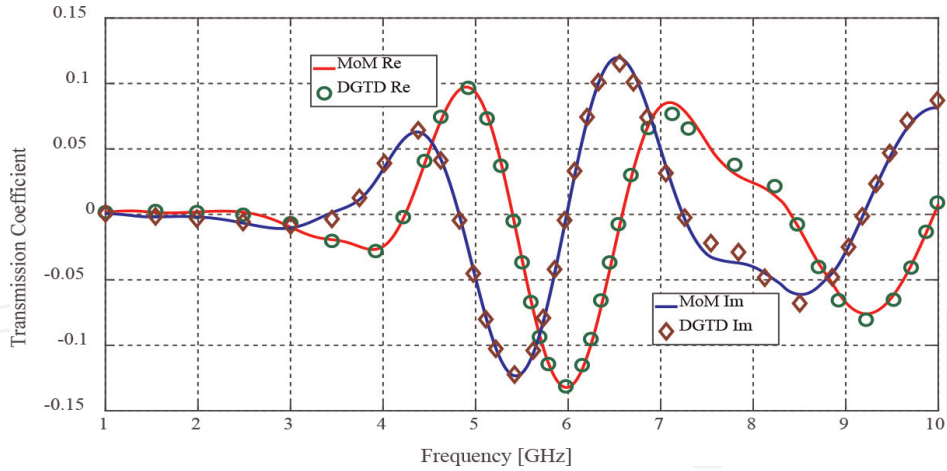


Figure 11. Transmission coefficient between the waveguide ports of the antenna array for the same permittivities $\epsilon_{r1} = \epsilon_{r2} = 2.25$, but different outer radii: $D_1/2 = 3.49$ mm, $D_2/2 = 6.52$ mm.

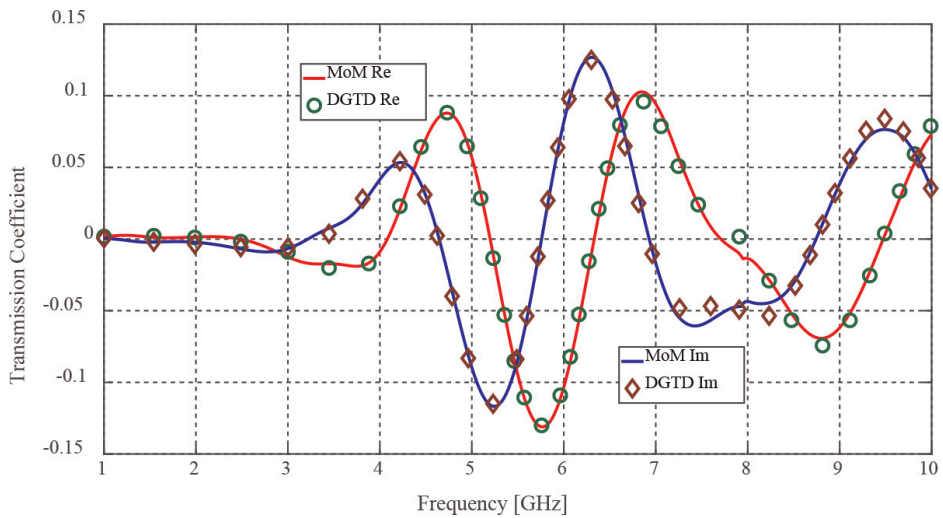


Figure 12. Transmission coefficient between the waveguide ports of the antenna array for the same outer radii $D_1/2 = D_2/2 = 5.3$ mm, but different permittivities: $\epsilon_{r1} = 4$ and $\epsilon_{r2} = 1.78$.

Figures 11 and 12 show a comparison of the transmission coefficient $S_{21} = a_{02}^-/a_{01}^+ \sqrt{Z_{c1}/Z_{c2}}$ between waveguide ports 1 and 2, calculated by the MoM and DGTD method for different parameters of coaxial waveguides. Figure 11 is made for the same fillings of waveguides: $\epsilon_{r1} = \epsilon_{r2} = 2.25$, but with different outer radii: $D_1/2 = 3.49$ mm and $D_2/2 = 6.52$ mm, while Figure 12 is performed for different fillings: $\epsilon_{r1} = 4$ and $\epsilon_{r2} = 1.78$, but with the same outer radii $D_1/2 = D_2/2 = 5.3$ mm. Both cases result in characteristic impedances of waveguides $Z_{c1} = 50 \Omega$ and $Z_{c2} = 75 \Omega$. Comparison of the MoM and DGTD results again shows very good agreement between both simulated results, which validates the developed approach to modeling coupling problems for coaxial waveguide ports with different characteristic impedances.

5. Application of waveguide port approach

The obtained approach has been applied to practical EMC problems for microwave antennas fed by coaxial waveguides. Such waveguides are the most commonly used to

excite microwave antennas and electronic devices. This excitation usually uses microwave coaxial connectors, such as BNC and SMA.

5.1 Modeling of two branches feeding large printed UWB antenna

First, based on the measurement data [28], a printed ultra-wideband (UWB) antenna is considered. **Figure 13** shows a schematic view of a large printed UWB antenna with a two-branch-feed, the bottom of which is connected to the core of a 50 Ω SMA connector with waveguide excitation, the covering of which is connected to a metal plate serving as a reflector. The bottom end of the connector is accepted as a waveguide port, and the input impedance of the UWB antenna at the waveguide port is measured and simulated.

The model of a printed UWB antenna is a square metal patch with a length $L_a = 40$ mm and a width $W_a = 40$ mm, printed on a dielectric substrate with a length $L_b = 43$ mm, a width $W_b = 47.5$ mm, a thickness $t = 1.5$ mm and material parameters $\epsilon_{rd} = 4.4$ and $\tan\delta_d = 0.02$. The antenna is connected to a two-branch-feeding strip with a total width $t_1 = 15$ mm, a distance between the branches $t_2 = 11$ mm, and a height of the branches $h_1 = 3.5$ mm. The UWB antenna is placed at a height $h_2 = 3$ mm above a metallic plate of a length $L = 275$ mm and a width $W = 207$ mm and is connected to the SMA connector. The model of the SMA connector is represented by a coaxial waveguide with an outer radius $D/2 = 2.125$ mm, inner radius $d/2 = 0.635$ mm, and a length $L_{con} = 6.8$ mm, filled with a polyethylene dielectric with relative permittivity $\epsilon_r = 2.24$ and loss tangent $\tan \delta = 0.005$.

Figure 14 shows a comparison of simulated input impedances of a printed UWB antenna at the waveguide port with measurement results [28]. Comparison of the simulated results with measurement data shows a good agreement between them in a wide frequency range from 1 to 10 GHz. This validates the developed approach to modeling the composite antenna geometries fed by coaxial waveguides with dielectric filling.

5.2 Coupling problem between GPS and SDARS antennas

In conclusion, based on the measurement data [28], the coupling between the GPS and SDARS patch antennas was analyzed in the frequency range from 1 GHz to 3 GHz. **Figure 15** shows the measurement setup (a) and its schematic view (b) for studying

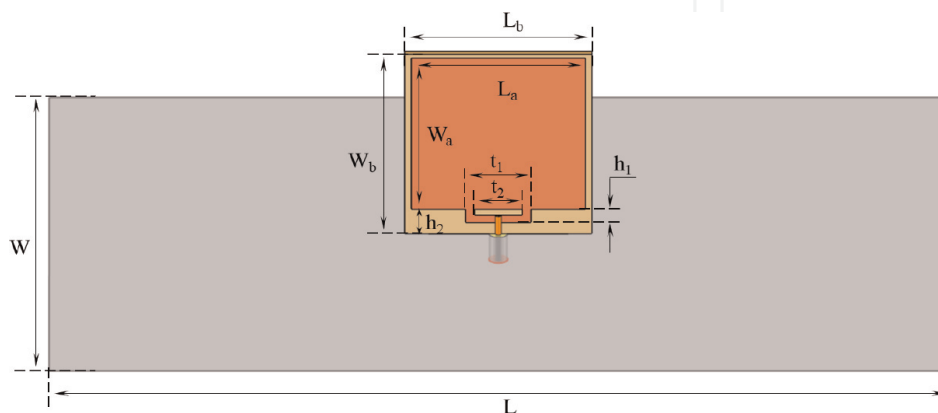


Figure 13. Schematic view of a large printed UWB antenna with two branch feed connected to a coaxial waveguide port.

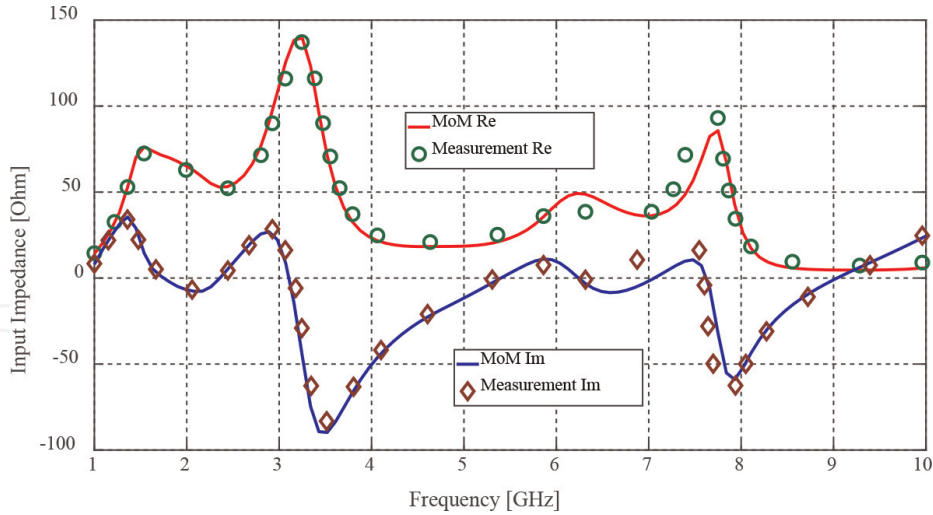


Figure 14. Comparison of the simulated and measured input impedances of a printed UWB antenna.

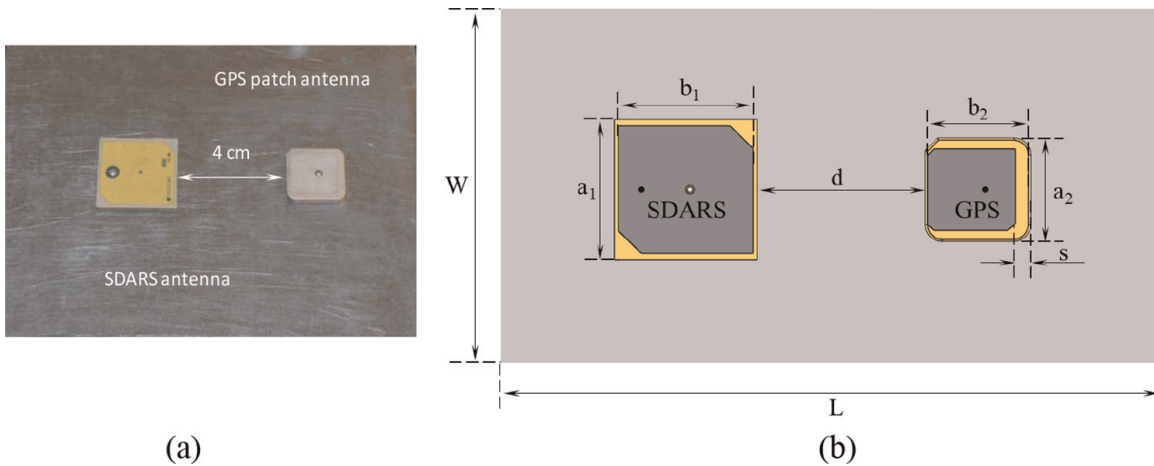


Figure 15. Measurement setup (a) and its schematic view (b) for the coupled GPS and SDARS patch antennas.

the coupling between active GPS and passive SDARS antennas, separated by a distance of $d = 4$ cm. Both antennas are fed by 50 Ohm coaxial lines with standard SMA connectors with parameters described in Section 5.1.

The parameters of the setup are the following. The SDARS antenna is a square metallic patch of $32 \text{ mm} \times 32 \text{ mm}$ size with two opposite cut corners, printed on a dielectric substrate with dimensions $34 \text{ mm} \times 34 \text{ mm} \times 3.25 \text{ mm}$ and $\epsilon_r = 4.1$. The GPS antenna is constructed by a square metallic patch of $21 \text{ mm} \times 21 \text{ mm}$ size with truncated corners, printed on a $25 \text{ mm} \times 25 \text{ mm} \times 4 \text{ mm}$ dielectric substrate with $\epsilon_{r1} = 20.34$. Both patch antennas are mounted on a $190 \text{ mm} \times 145 \text{ mm}$ metal plate.

Figure 16 shows a comparison of the transmission coefficient between active GPS and passive SDARS patch antennas, obtained by the developed MoM approach and measurements. A pretty good agreement between the simulated results and measured data in the frequency range of 1–3 GHz is observed. This comparison validates the developed waveguide port approach with measurements to model coupling problems between different composite geometry antennas with coaxial waveguide ports.

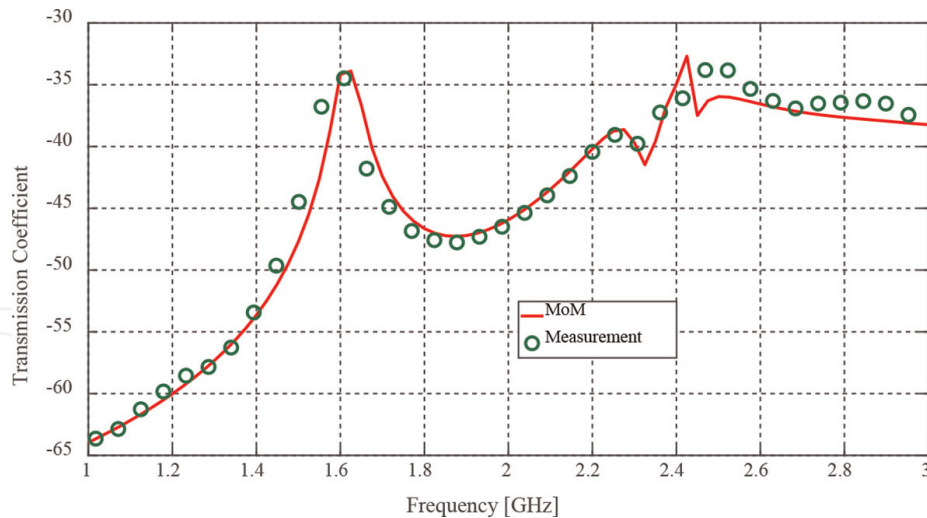


Figure 16.
Transmission coefficient between GPS and SDARS patch antennas.

6. Conclusion


The MoM-based waveguide port approach was developed to model waveguide port excitation problems on arbitrary conducting and composite geometries. The developed approach was validated for modeling radiation and coupling problems for coaxial ports by comparing the simulated results with those obtained by other approaches and measurements. The approach has been applied to practical EMC problems for microwave antennas fed by coaxial connectors. A good agreement between the simulated and measured results has been demonstrated. The efficiency of the developed approach for solving various complex problems with waveguide excitation has been verified.

Author details

Faik Bogdanov*, Irina Chochia, Lily Svanidze and Roman Jobava
EMCoS LLC, Tbilisi, Georgia

*Address all correspondence to: faik.bogdanov@emcos.com

IntechOpen

© 2022 The Author(s). Licensee IntechOpen. This chapter is distributed under the terms of the Creative Commons Attribution License (<http://creativecommons.org/licenses/by/3.0>), which permits unrestricted use, distribution, and reproduction in any medium, provided the original work is properly cited. 

References

- [1] Lou Z, Jin JM. An accurate waveguide port boundary condition for the time-domain finite-element method. *IEEE Transactions on Microwave Theory and Techniques*. 2005;**53**(9):3014-3023. DOI: 10.1109/APS.2005.1551498
- [2] Jin JM, Riley DJ. *Finite Element Analysis of Antennas and Arrays*. Hoboken: Wiley; 2008. 467p
- [3] Alimenti F, Mezzanotte P, Roselli L, Sorrentino R. Modal absorption in the FDTD method: A critical review. *International Journal of Numerical Model*. 1997;**10**:245-264
- [4] Alimenti F, Mezzanotte P, Roselli L, Sorrentino R. A revised formulation of modal absorbing and matched modal source boundary conditions for the efficient FDTD analysis of waveguide structures. *IEEE Transactions on Microwave Theory and Techniques*. 2000;**48**(1):50-59. DOI: 10.1109/22.817471
- [5] Flisgen T, Heller J, Rienen U. Time-domain absorbing boundary terminations for waveguide ports based on state-space models. *IEEE Transactions on Magnetics*. 2014;**50**(2): 145-148. DOI: 10.1109/TMAG.2013.2283065
- [6] Li P, Jiang LJ, Bađci H. Transient analysis of dispersive power-ground plate pairs with arbitrarily shaped antipads by the DGTD method with wave port excitation. *IEEE Transactions on Electromagnetic Compatibility*. 2017;**59**(1):172-183
- [7] Štumpf M, Šeděnka V, Kadlec P. On modeling of excitation ports in the time-domain contour-integral method. In: *Proceedings of the International Conference on Electromagnetics in Advanced Applications (ICEAA'17)*; 11–15 September 2017; Verona, Italy. IEEE; 2017. pp. 1292-1294. DOI:10.1109/ICEAA.2017.8065509
- [8] Harrington RF. *Field Computation by Moment Methods*. New York: Macmillan; 1968
- [9] Harrington RF, Mautz JR. A generalized network formulation for aperture problems. *IEEE Transactions on Antennas and Propagation*. 1976;**24**(6): 870-873. DOI: 10.1109/TAP.1976.1141420
- [10] Wang T, Harrington R, Mautz JR. Electromagnetic scattering from and transmission through arbitrary apertures in conducting bodies. *IEEE Transactions on Antennas and Propagation*. 1990;**38**(11):1805-1814. DOI: 10.1109/8.102743
- [11] Bunger R. Moment-method analysis of arbitrary 3-D metallic N-port waveguide structures. *IEEE Transactions on Microwave Theory and Techniques*. 2000;**48**(4):531-537
- [12] Wen D, Chen H, Zhang J. *Radiation Characteristic Analysis of Ridged Horn by Aperture Port Excitation*. Xi'an, China: IEEE; 2012. pp. 759-761
- [13] Bogdanov F, Chochia I, Svanidze L, Jobava R. Incorporation of MoM-based waveguide port model into the mixed conducting and dielectric geometry. In: *Proceedings of the International Symposium on Electromagnetic Compatibility (EMC Europe'17)*; 4–8 September 2017; Angers, France. IEEE; 2017. pp. 1-6. DOI:10.1109/EMCEurope.2017.8094718
- [14] Bogdanov F, Svanidze L, Gheonjian A, Eremyan D, Kut Chadze Z, Jobava R.

Application of MoM-based waveguide port approach to the analysis of EM coupling problems related to microwave antennas. In: Proceedings of the European Conference on Antennas and Propagation (EUCAP'18); 9–13 April 2018; London, England. IEEE; 2018. pp. 1-5. DOI:10.1049/cp.2018.1194

[15] Bogdanov F, Chochia I, Svanidze L, Jobava R. Validation of MoM-based solution of waveguide port problem for composite structures applied to microwave antenna and PCB geometries. In: Proceedings of the European Microwave Conference (EuMC'19); 1–3 October 2019; Paris, France. IEEE; 2019. pp. 642-645. DOI:10.23919/EuMC.2019.8910683

[16] Arvas E, Rahhal-Arabi A, Sadigh A, Rao SM. Scattering from multiple conducting and dielectric bodies of arbitrary shape. *IEEE Antennas and Propagation Magazine*. 1991;33(2):29-36. DOI: 10.1109/74.88184

[17] Goggans PM, Kishk AA, Glisson AW. Electromagnetic scattering from objects composed of multiple homogeneous regions using a region-by-region solution. *IEEE Transactions on Antennas and Propagation*. 1994;42(6):865-871. DOI: 10.1109/8.301713

[18] Shin J, Glisson AW, Kishk AA. Analysis of combined conducting and dielectric structures of arbitrary shapes using an E-PMCHW integral equation formulation. In: Proceedings of IEEE-AP-S Symposium (AP-S'00). Vol. 4. 2000. pp. 2282-2285

[19] Kolundzija BM. Electromagnetic modeling of composite metallic and dielectric structures. *IEEE Transactions on Microwave Theory and Techniques*. 1999;47(7):1021-1032

[20] Yiäa-Oijala P, Taskinen M, Sarvas J. Surface integral equation method for general composite metallic and dielectric structures with junctions. *Progress In Electromagnetics Research*. 2005;52: 81-108. DOI: 10.2528/PIER04071301

[21] Carr M, Topsakal E, Volakis JL. A procedure for modeling material junctions in 3-D surface integral equation approaches. *IEEE Transactions on Antennas and Propagation*. 2004; 52(5):1374-1379. DOI: 10.1109/TAP.2004.827247

[22] Bogdanov F, Svanidze L, Jobava R. MoM solution to scattering problem on multi-region composite structures with various type material junctions. In: Proceedings of International Seminar/ Workshop (DIPED'18); 24–27 September 2018; Tbilisi. pp. 13-18. DOI:10.1109/DIPED.2018.8543281

[23] EMCoS. EMCoS Studio 2021 [Internet]. Available from: <http://www.emcos.com>

[24] Harrington RF. *Time-Harmonic Electromagnetic Fields*. New York: McGraw-Hill; 1961

[25] Cho YH. Analytic and numerically efficient scattering equations for an infinitely flanged coaxial line. *PIERS Letters*. 2012;28:149-158. DOI: 10.2528/PIERL11110901

[26] Tan W, Shen Z. Efficient analysis of open-ended coaxial line using Sommerfeld identity and matrix pencil method. *IEEE Microwave and Wireless Components Letters*. 2008;18(1):7-9. DOI: 10.1109/LMWC.2007.911971

[27] Mosig JR, Besson JE, Gex-Fabry M, Gardiol FE. Reflection of an open-ended coaxial line and application to non-destructive measurement of materials. *IEEE Transactions on Instrumentation*

and Measurement. 1981;**30**(1):46-51.
DOI: 10.1109/TIM.1981.6312437

[28] Eremyan D, Kutchadze Z, Badzagua I, Gheonjian A, Jobava R. Validation of discontinuous Galerkin method. EMCoS Internal Report. Tbilisi, Georgia; 2013

IntechOpen

IntechOpen